



UNIVERSITY  
OF WOLLONGONG  
AUSTRALIA

University of Wollongong  
Research Online

---

Australian Institute for Innovative Materials - Papers

Australian Institute for Innovative Materials

---

2016

# Ambient synthesis of one-/two-dimensional CuAgSe ternary nanotubes as counter electrodes of quantum-dot-sensitized solar cells

Xin Qi Chen

*University of Wollongong*

Yang Bai

*University of Queensland*

Zhen Li

*University of Wollongong, zhenl@uow.edu.au*

Lian Zhou Wang

*University of Queensland*

S X. Dou

*University of Wollongong, shi@uow.edu.au*

---

## Publication Details

Chen, X., Bai, Y., Li, Z., Wang, L. & Dou, S. Xue. (2016). Ambient synthesis of one-/two-dimensional CuAgSe ternary nanotubes as counter electrodes of quantum-dot-sensitized solar cells. *ChemPlusChem*, 81 (4), 414-420.

Research Online is the open access institutional repository for the University of Wollongong. For further information contact the UOW Library:  
[research-pubs@uow.edu.au](mailto:research-pubs@uow.edu.au)

---

# Ambient synthesis of one-/two-dimensional CuAgSe ternary nanotubes as counter electrodes of quantum-dot-sensitized solar cells

## Abstract

2015 WILEY-VCH Verlag GmbH & Co. KGaA, Weinheim. One-/two-dimensional ternary CuAgSe nanotubes (NTs) were successfully prepared from copper selenide ( $\text{Cu}_{2-x}\text{Se}$ ) NTs at room temperature within a short reaction time by the facile cation-exchange approach. Cation exchange leads to the transformation of the crystal structure from cubic into orthorhombic and/or tetragonal with good retention of morphology. The exchange reactions are spontaneous owing to large negative changes of the Gibbs free energy. The effects of parameters such as reaction time, precursor source, and precursor ratio on the exchange reaction were investigated. The resultant CuAgSe NTs were explored as counter electrodes (CEs) of quantum-dot-sensitized solar cells (QDSSCs) and achieved higher conversion efficiency ( $\eta=5.61\%$ ) than those of QDSSCs with the gold as the CE (3.32%).

## Keywords

ambient, cells, solar, sensitized, dot, quantum, electrodes, counter, nanotubes, ternary, cuagse, dimensional, two, one, synthesis

## Disciplines

Engineering | Physical Sciences and Mathematics

## Publication Details

Chen, X., Bai, Y., Li, Z., Wang, L. & Dou, S. Xue. (2016). Ambient synthesis of one-/two-dimensional CuAgSe ternary nanotubes as counter electrodes of quantum-dot-sensitized solar cells. *ChemPlusChem*, 81 (4), 414-420.

# Ambient Synthesis of One-/Two-Dimensional CuAgSe Ternary Nanotubes as Counter Electrodes of Quantum-Dot-Sensitized Solar Cells

Xin Qi Chen,<sup>[a, d]</sup> Yang Bai,<sup>[c]</sup> Zhen Li,<sup>\*[a, b]</sup> Lian Zhou Wang,<sup>[c]</sup> and Shi Xue Dou<sup>[a]</sup>

One-/two-dimensional ternary CuAgSe nanotubes (NTs) were successfully prepared from copper selenide (Cu<sub>2-x</sub>Se) NTs at room temperature within a short reaction time by the facile cation-exchange approach. Cation exchange leads to the transformation of the crystal structure from cubic into orthorhombic and/or tetragonal with good retention of morphology. The exchange reactions are spontaneous owing to large negative

changes of the Gibbs free energy. The effects of parameters such as reaction time, precursor source, and precursor ratio on the exchange reaction were investigated. The resultant CuAgSe NTs were explored as counter electrodes (CEs) of quantum-dot-sensitized solar cells (QDSSCs) and achieved higher conversion efficiency ( $\eta = 5.61\%$ ) than those of QDSSCs with the gold as the CE (3.32%).

## Introduction

One-/two-dimensional (1D/2D) ternary semiconductor nanotubes (NTs) have been the subject of extensive studies not only because their electronic structures and properties can be engineered over a broad range for diverse applications such as photodetectors,<sup>[1,2]</sup> photovoltaics,<sup>[3]</sup> and electronics,<sup>[4]</sup> but also because their unique morphology consists of internal tubes and external nanosheets to form a large surface area, which enables them to be good electron transporters and show better performance than that of solid analogues.<sup>[5]</sup> For example, ternary CuAgSe has high mobility from both Cu<sup>+</sup> and Ag<sup>+</sup>

ions, and displays better performance than binary Ag<sub>2</sub>Se or Cu<sub>2</sub>Se in electrochemical devices.<sup>[6-8]</sup> This material was initially reported in the 1950s,<sup>[9,10]</sup> and has been rarely studied owing to difficulties in synthesis, especially for the preparation of nanostructures. Ternary CuAgSe is conventionally synthesized by heating a mixture of Ag, Cu, and Se powder to over 1000 K with several heating and cooling steps.<sup>[11,12]</sup> Thin CuAgSe films can be prepared by the electrodeposition method.<sup>[13]</sup> The crystal size of the products generated by these methods is quite large and uncontrollable, and recent advances in nanofabrication have led to new insights into the preparation and application of ternary CuAgSe nanostructures. For example, surfactant-free CuAgSe nanoparticles were prepared on a large scale to show the temperature-dependent reversible transition of metallic *n-p* conductivity, and great potential in converting heat into electricity through the Seebeck effect.<sup>[14]</sup> Both dendritic and tubular CuAgSe were prepared from Ag<sub>2</sub>Se/Ag or Ag<sub>2</sub>Se/Se templates,<sup>[6,15]</sup> but it was time consuming and difficult to avoid Ag or Se in the final products. Thus, a facile and efficient method for the synthesis of ternary CuAgSe nanomaterials with well-defined composition and architecture is desirable.

Compared with the aforementioned approaches, cation exchange has emerged as a particularly powerful and promising method to prepare well-defined nanoarchitectures.<sup>[16-20]</sup> It offers a new avenue to create chemically and compositionally diverse nanomaterials, and is particularly suitable for the preparation of late-transition-metal chalcogenide nanostructures.<sup>[21-23]</sup> This strategy has been successfully applied to prepare heterostructured, doped, alloyed, hollow, and core-shell nanocrystals; nanorods; and nanowires.<sup>[17,24-29]</sup> For example, a dual-interface heterostructured copper sulfide layer capped with zinc sulfide grains in spherical nanocrystals were synthesized, and the extent of cation exchange could be precisely manipulated to tune the thickness of the internal layer down

[a] X. Q. Chen, Prof. Z. Li, Prof. S. X. Dou  
Institute for Superconducting and Electronic Materials, Squires Way  
Innovation Campus of the University of Wollongong  
Wollongong, 2500, New South Wales (Australia)  
Fax: (+61)2-42215731  
E-mail: zhenl@uow.edu.au  
zhenli@suda.edu.cn

[b] Prof. Z. Li  
School of Radiation Medicine and Radiation Protection  
Collaborative Innovation Center of Radiation Medicine  
of Jiangsu Higher Education Institutions  
Soochow University, 199 Ren Ai Road, Suzhou Industrial Park  
Suzhou 215123 (P.R. China)

[c] Dr. Y. Bai, Prof. L. Z. Wang  
Nanomaterials Centre, School of Chemical Engineering and Australian  
Institute for Bioengineering and Nanotechnology (AIBN)  
University of Queensland, QLD 4072 (Australia)

[d] X. Q. Chen  
Institute of Nanoscience and Nanotechnology  
Department of Physics, Central China Normal University  
Wuhan, 430079 (P.R. China)

Supporting information for this article is available on the WWW under <http://dx.doi.org/10.1002/cplu.201500466>. It contains low-magnification the SEM image and EDX pattern of CuAgSe NTs, XRD patterns of CuSe and Ag<sub>2</sub>Se, XRD patterns of the products prepared from different molar ratios of Cu<sub>2-x</sub>Se to AgNO<sub>3</sub>, XRD patterns and SEM images of CuAgSe NTs, and XPS spectra of Ag 3d in the samples prepared from silver acetate and collected after different reaction times.

to the single-atom level.<sup>[17]</sup> Hollow and cave-shaped nanoparticles of  $\text{Cu}_{2-x}\text{S}_y\text{Se}_{1-y}$  were prepared from core-shell  $\text{Cu}_{2-x}\text{Se}/\text{Cu}_{2-x}\text{S}$  nanocrystals by the diffusion of  $\text{Cu}^+$  from the  $\text{Cu}_{2-x}\text{Se}$  core into the  $\text{Cu}_{2-x}\text{S}$  shell.<sup>[29]</sup> Recently, phase-selective cation exchange enabled the successful transition of CdS nanowires into  $\text{Cu}_{2-x}\text{S}$  nanowires with tunable crystal structures.<sup>[28]</sup> Owing to complications of partial or complete cation exchange between binary compounds, very few reports are available on the preparation of hierarchical 1D/2D ternary CuAgSe NTs.

In this study, we synthesized 1D/2D ternary CuAgSe NTs from  $\text{Cu}_{2-x}\text{Se}$  NTs through the facile cation-exchange method at room temperature with a short reaction time. The resultant CuAgSe NTs were employed as the counter electrodes (CEs) of quantum-dot-sensitized solar cells (QDSSCs) to generate a conversion efficiency ( $\eta$ ) of 5.61%. To the best of our knowledge, this is the first report on 1D/2D ternary CuAgSe NTs and their application in QDSSCs.

## Results and Discussion

The 1D/2D ternary CuAgSe NTs were fabricated by cation exchange from freshly prepared  $\text{Cu}_{2-x}\text{Se}$  NTs reacted with a solution of  $\text{AgNO}_3$  in ethanol. Typical field-emission (FE) SEM and TEM images of the initial  $\text{Cu}_{2-x}\text{Se}$  NTs show their 1D/2D morphology with an inner diameter of 300 nm and an outer diameter of 600 nm, on average (Figure 1a, b). After partial exchange of copper ions with silver ions, the nanosheets on the surfaces of the resultant CuAgSe NTs become smaller (Figure 1d, e) and the 1D/2D tubular structure is retained (Figure S1 in the Supporting Information). The HRTEM images clearly display continuous lattice fringes with spacings of 0.33 and 0.2 nm (Figure 1c, f), which match well with those of the (111) planes of  $\text{Cu}_{2-x}\text{Se}$  and the (152) planes of CuAgSe, respectively. The FFT patterns also support the transition of the crys-

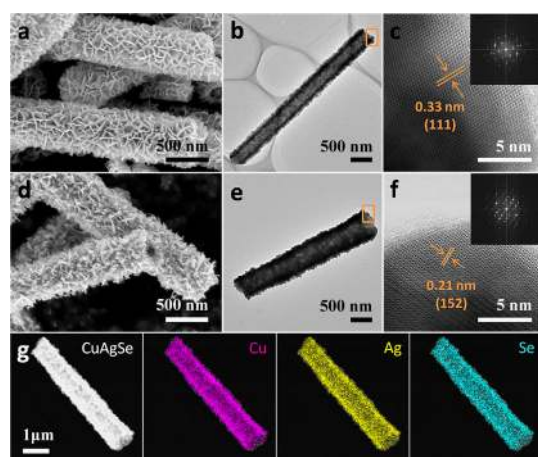


**Figure 1.** FESEM images of the  $\text{Cu}_{2-x}\text{Se}$  NTs (a) and resultant CuAgSe NTs (d). TEM images of  $\text{Cu}_{2-x}\text{Se}$  NT (b) and CuAgSe NT (e). c, f) High-resolution (HR) TEM images of the selected areas in (b) and (e), respectively. The insets contain fast Fourier transform (FFT) patterns of the HRTEM images. g) Scanning transmission electron microscopy (STEM) image and energy-dispersive X-ray spectroscopy (EDX) elemental mapping of Cu, Ag, and Se for a typical CuAgSe NT.

tal structure after cation exchange. A STEM image and the corresponding EDX elemental mapping images of a single CuAgSe NT are shown in Figure 1g; these results reveal the homogeneous distribution of Cu, Ag, and Se throughout the whole NT. The EDX spectrum of an individual CuAgSe NT (Figure S2 in the Supporting Information) further confirms the presence of these elements with a ratio of 1.46/1.1/1, which is consistent with that (1.22/1/1.04) determined by inductively coupled plasma atomic emission spectroscopy (ICP-AES).

The transformation of  $\text{Cu}_{2-x}\text{Se}$  NTs into CuAgSe NTs is also proved by the XRD patterns (Figure 2). The diffraction peaks in the orange pattern in Figure 2 match well with orthorhombic CuAgSe (JCPDS 10-0451) and tetragonal CuAgSe (JCPDS 25-1180), which are different from those of the cubic structure of  $\text{Cu}_{2-x}\text{Se}$  (JCPDS 88-2043; Figure 3). It should be noted that there is no big difference between these two structures, except that the orthorhombic structure features a sequence that repeats itself periodically every five tetragonal cells in the *b* direction.<sup>[14]</sup> They have similar layered structures with alternating stacking of the Ag and CuSe layers, in which Ag atoms almost lie in the same plane and are bonded closely to Se atoms, which allows high mobility of Ag atoms and the formation of Ag–Ag metallic bonds. Selenium atoms form a squashed tetrahedron, in which each corner is shared with an adjacent tetrahedron, and copper atoms are offset from the center within the tetrahedron.<sup>[10]</sup>

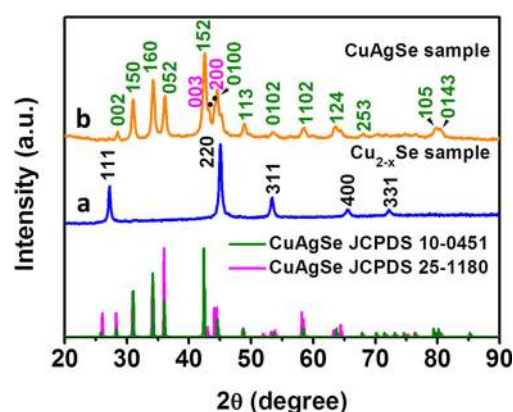


**Figure 2.** XRD patterns of a)  $\text{Cu}_{2-x}\text{Se}$  NTs and b) CuAgSe NTs with standard XRD peaks.

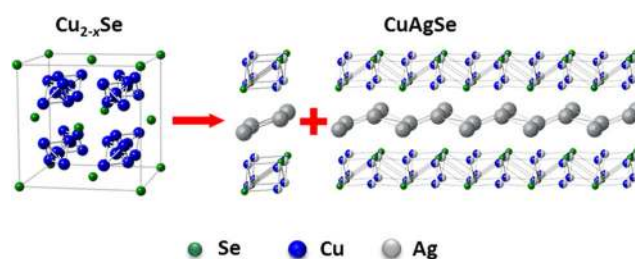


**Figure 3.** Structure diagrams of cubic  $\text{Cu}_{2-x}\text{Se}$ , and tetragonal and orthorhombic CuAgSe unit cells.

Because stoichiometric  $\text{Cu}_2\text{Se}$  is easily oxidized into nonstoichiometric  $\text{Cu}_{2-x}\text{Se}$ ,<sup>[30]</sup> X-ray photoelectron spectroscopy (XPS) was used to determine the valence states of elements in both  $\text{Cu}_{2-x}\text{Se}$  and  $\text{CuAgSe}$  NTs (Figure 4). The spectra of  $\text{Cu}$  2p confirm the presence of both  $\text{Cu}^+$  and  $\text{Cu}^{2+}$  (with a calculated ratio of 3.16) in  $\text{Cu}_{2-x}\text{Se}$  NTs, from which the  $\text{Cu}^{2+}$  ions were completely transformed into  $\text{Cu}^+$  in  $\text{CuAgSe}$  NTs after cation exchange, as evidenced by the disappearance of the characteristic peak of  $\text{Cu}^{2+}$  at around 942 eV. Two peaks at 373.2 and 367.6 eV of  $\text{Ag}$  3d in the product indicate the absence of other  $\text{Ag}$  species. The binding energy of  $\text{Se}$  3d<sub>3/2</sub> at 53.7 eV corresponds to  $\text{Se}^{2-}$  in both  $\text{Cu}_{2-x}\text{Se}$  and  $\text{CuAgSe}$  NTs, and the small peak at 58.2 eV in the  $\text{Cu}_{2-x}\text{Se}$  sample is attributed to surface-adsorbed  $\text{Se}$  (the ratio of  $\text{Se}^{2-}$  to  $\text{Se}^0$  in  $\text{Cu}_{2-x}\text{Se}$  was calculated to be 3.33).<sup>[14,31–33]</sup>

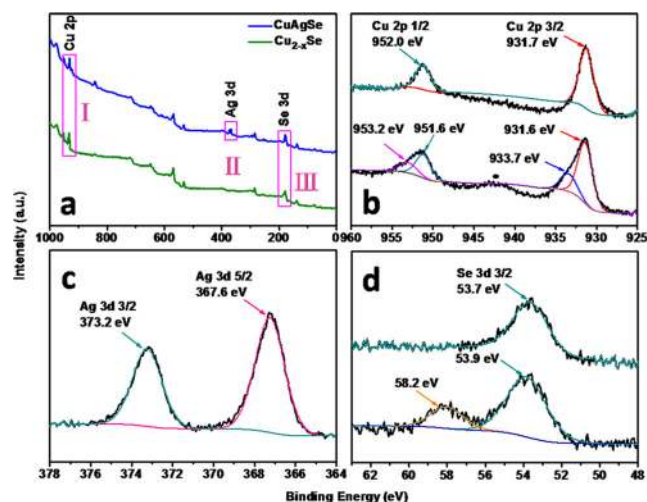


**Figure 4.** XPS spectra of  $\text{Cu}_{2-x}\text{Se}$  and  $\text{CuAgSe}$  NTs: a) survey spectra; b)  $\text{Cu}$  2p spectra of area I in (a), with the black dot marking the satellite peak of  $\text{Cu}^{2+}$ ; c)  $\text{Ag}$  3d spectrum of area II in (a); and d)  $\text{Se}$  3d spectra of area III in (a).

The exchange reaction was investigated by analyzing the intermediate products collected after different reaction times. Figure 5a shows the XRD patterns of samples collected at 1, 2, 10, and 20 min during the exchange reaction. When a solution of  $\text{Cu}_{2-x}\text{Se}$  in ethanol was reacted with a solution of  $\text{AgNO}_3$  in ethanol for 1 min, the product obtained was a mixture of  $\text{CuAgSe}$ ,  $\text{Ag}_2\text{Se}$ , and a small amount of  $\text{Ag}$ . This result demonstrates the fast exchange reaction between copper and silver ions, which is attributed to their strong mobility and capability for diffusion into/out of the lattice.<sup>[7]</sup> After reaction for 2 min, the product was still composed of these three compounds, but the amount of  $\text{Ag}_2\text{Se}$  and  $\text{Ag}$  decreased, as indicated by the lower intensity of the peaks in the XRD patterns. The intermediate sample collected at 10 min was a mixture of  $\text{CuAgSe}$  and  $\text{Ag}_2\text{Se}$ , and the peak corresponding to  $\text{Ag}$  disappeared or was not detectable. The final product collected at 20 min was pure  $\text{CuAgSe}$ , which demonstrated the complete transformation of  $\text{Cu}_{2-x}\text{Se}$  NTs into  $\text{CuAgSe}$  NTs. The transformation was also supported by XPS spectra of  $\text{Ag}^+$  and  $\text{Ag}^0$  in all samples

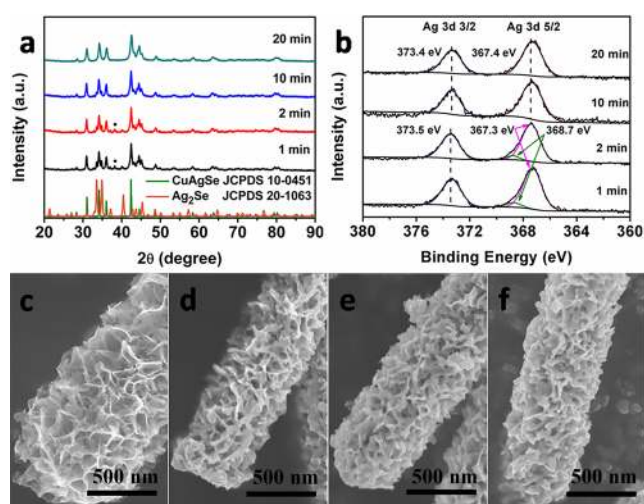
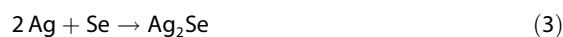
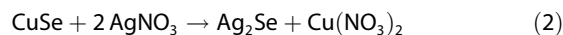


**Figure 5.** a) XRD patterns of products and b) XPS spectra of  $\text{Ag}$  3d from samples collected at different reaction times. The diffraction peaks marked with black dots arise from  $\text{Ag}$ . SEM images of NTs collected at c) 1, d) 2, e) 10, and f) 20 min.

collected at different reaction times (Figure 5b). Within the initial 2 min,  $\text{Ag}$  3d<sub>5/2</sub> peaks in the collected samples can be fitted into two peaks at 368.7 ( $\text{Ag}^0$ ) and 367.3 eV ( $\text{Ag}^+$ ). The  $\text{Ag}^0/\text{Ag}^+$  ratios in the samples collected at 1 and 2 min decreased from 12.83 to 10.48, which meant that there was conversion of  $\text{Ag}^0$  into  $\text{Ag}^+$  as the reaction time was extended. When the mixture was reacted for 10 min, the absence of any  $\text{Ag}^0$  peak suggested that all  $\text{Ag}$  formed was completely converted. The evolution of the morphology during cation exchange was monitored by SEM (Figure 5c–f). There is no big difference in the morphologies, except that the surface nano-sheets became thicker and rougher with increasing reaction time.

From the perspective of the molecular formula,  $\text{Cu}_{2-x}\text{Se}$  ( $0 \leq x \leq 1$ ) could be considered as a mixture of  $\text{CuSe}$  and  $\text{Cu}_2\text{Se}$ , and the transformation of  $\text{Cu}_{2-x}\text{Se}$  into  $\text{CuAgSe}$  could be treated as their reactions with  $\text{AgNO}_3$  [Eqs. (1) and (2)].  $\text{Cu}_2\text{Se}$  could react with  $\text{AgNO}_3$  to form  $\text{CuAgSe}$ ,  $\text{Ag}$ , and  $\text{Cu}(\text{NO}_3)_2$  through the redox reactions between  $\text{Cu}^+$ ,  $\text{Ag}^+$ , and  $\text{NO}_3^-$ , as evidenced by the XRD and XPS results.  $\text{CuSe}$  reacted with  $\text{AgNO}_3$  to form  $\text{Ag}_2\text{Se}$  owing to its greater solubility ( $K_{\text{sp}}(\text{CuSe}) = 7.94 \times 10^{-49}$ ) than that of  $\text{Ag}_2\text{Se}$  ( $K_{\text{sp}}(\text{Ag}_2\text{Se}) = 2.0 \times 10^{-64}$ ), which was proved by mixing a solution of pure  $\text{CuSe}$  in ethanol with a solution of  $\text{AgNO}_3$  in ethanol at room temperature to form  $\text{Ag}_2\text{Se}$  (Figure S3 in the Supporting Information). The characteristic blue solution suggests the formation of  $\text{Cu}(\text{NO}_3)_2$  during exchange reactions. Thus-formed  $\text{Ag}$  reacted with residual  $\text{Se}$  (adsorbed by  $\text{Cu}_{2-x}\text{Se}$  NTs) to form  $\text{Ag}_2\text{Se}$  [Eq. (3)], which further reacted with  $\text{Cu}_2\text{Se}$  to form  $\text{CuAgSe}$  [Eq. (4)].<sup>[14]</sup> To demonstrate these reactions, the effects of the molar ratio of  $\text{Cu}_{2-x}\text{Se}$  NTs to  $\text{AgNO}_3$  in the product were investigated. In the cases of more  $\text{Cu}_{2-x}\text{Se}$  NTs (i.e.,  $\text{Cu}_{2-x}\text{Se}/\text{AgNO}_3 = 2.5/1$  or  $1.5/1$ ), there is insufficient  $\text{AgNO}_3$  for the reactions and the main product is  $\text{Cu}_{2-x}\text{Se}$ , which is labeled with \* in Figure S4 in the Supporting Information. In the opposite

cases (i.e.,  $\text{Cu}_{2-x}\text{Se}/\text{AgNO}_3 = 1/2$  or  $1/3$ ), excess  $\text{AgNO}_3$  leads to the formation of Ag (marked with  $\Delta$  in Figure S4 in the Supporting Information). Therefore, it is crucial to control the molar ratio of  $\text{Cu}_{2-x}\text{Se}/\text{AgNO}_3$ ; the optimal ratio is 1/1.



These exchange reactions took place spontaneously as a result of three factors. First, the high mobility of  $\text{Cu}^{2+}$ ,  $\text{Cu}^+$ , and  $\text{Ag}^+$  ions and their strong capability for diffusion into/out of the lattice ensure fast reactions. The presence of copper vacancies also significantly accelerates the cation-exchange process at room temperature.<sup>[34]</sup> Second, the changes of Gibbs free energy ( $\Delta G$ ) for the reactions in Equations (1)–(4) are calculated to be  $-85.7$ ,  $-55.8$ ,  $-43.5$ , and  $-84.4 \text{ kJ mol}^{-1}$  based on the assumption that the reaction temperature is constant at 298 K and no entropy changes occur during the reaction. The standard  $\Delta_f H^\circ$  values at 298 K for  $\text{Cu}_2\text{Se}$ ,  $\text{CuSe}$ ,  $\text{Ag}_2\text{Se}$ ,  $\text{AgNO}_3$ ,  $\text{Cu}(\text{NO}_3)_2$ , and  $\text{CuAgSe}$  are  $-65.3$ ,  $-41.8$ ,  $-43.5$ ,  $-124.4$ ,  $-302.9$ , and  $-96.9 \text{ kJ mol}^{-1}$ , respectively.<sup>[6,7,35,36]</sup> Third, similar crystal structures of intermediate  $\text{Ag}_2\text{Se}$  and the  $\text{CuAgSe}$  product minimize the distortion of the crystal structure.

To better control the exchange process, we selected silver acetate to repeat the experiments and collected the intermediate products after different exchange times (i.e., 1, 2, 10, 20, and 60 min; Figures S5 and S6 in the Supporting Information). The results show that the complete transformation of  $\text{Cu}_{2-x}\text{Se}$  NTs into  $\text{CuAgSe}$  NTs took 60 min, owing to the lower dissociation capability of silver acetate in ethanol relative to that of  $\text{AgNO}_3$ . The same intermediate products ( $\text{Ag}_2\text{Se}$  and Ag) formed at an early stage (i.e., 1 and 2 min) and confirmed the same exchange process discussed above. Similar to the product prepared from  $\text{AgNO}_3$ , the morphology of  $\text{CuAgSe}$  NTs obtained from silver acetate is retained (Figure S7 in the Supporting Information).

As mentioned above, ternary  $\text{CuAgSe}$  might exhibit better electrochemical performance than that of its binary counterparts.<sup>[37]</sup> To evaluate the electrocatalytic activity, the resulting 1D/2D  $\text{CuAgSe}$  NTs were fabricated into CEs and then assembled with  $\text{CdS}/\text{CdSe}$  quantum dot (QD)-sensitized photoanodes to construct QDSSC devices containing polysulfide electrolyte. The electrocatalytic activities were compared with those of CEs fabricated from  $\text{Cu}_{2-x}\text{Se}$  NTs and Au under the same conditions.<sup>[38,39]</sup> The average photovoltaic performance parameters are provided in Table 1. Compared with the  $\text{Cu}_{2-x}\text{Se}$  NT and Au CEs, QDSSCs incorporating  $\text{CuAgSe}$  NT CEs delivered a larger  $J_{sc}$  value of  $17.57 \text{ mA cm}^{-2}$  (Figure 6a), which indicated the fast reduction of  $\text{S}_n^{2-}$  to  $n\text{S}^{2-}$ . In addition, the remarkable enhancement of the  $V_{oc}$  value of 581 mV, FF of 55.0%, can be ascribed to better electrical conductivity, and thus, suppressed charge

CEs	$V_{oc}$ [mV]	$J_{sc}$ [ $\text{mA cm}^{-2}$ ]	FF [%]	$\eta$ [%]	$R_s$ [ $\Omega$ ]	$R_{ct}$ [ $\Omega$ ]	$Z_w$ [ $\Omega$ ]
CuAgSe NT	581	17.57	55.0	5.61	10.8	0.67	4.17
$\text{Cu}_{2-x}\text{Se}$ NT	559	17.13	54.2	5.19	12.9	0.81	4.81
Au	507	13.34	49.1	3.32	16.0	42.43	72.13

[a]  $V_{oc}$  = open-circuit voltage,  $J_{sc}$  = short-circuit density, FF = fill factor,  $\eta$  = conversion efficiency,  $R_s$  = series resistance,  $R_{ct}$  = charge-transfer resistance,  $Z_w$  = Warburg diffusion impedance.

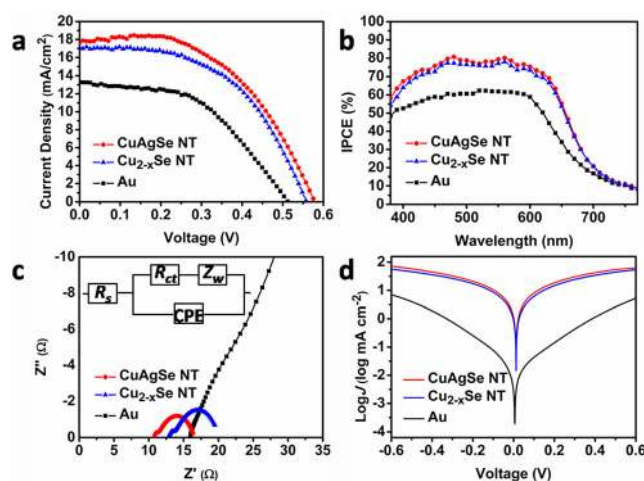


**Figure 6.** a) The photocurrent density–voltage ( $J$ – $V$ ) curves and b) incident photon-to-electron conversion efficiency (IPCE) spectra of QDSSCs with different CEs. c) Nyquist plots of the symmetrical dummy cells fabricated with three CEs; the inset shows the equivalent circuit. d) Tafel polarization of different dummy cells that were the same as those used for electrochemical impedance spectroscopy (EIS) measurements.

recombination. Figure 6b shows the IPCE spectra of typical QDSSCs based on three different CEs. Compared with both Au and  $\text{Cu}_{2-x}\text{Se}$  NT CEs, the IPCE profile of QDSSCs employing the  $\text{CuAgSe}$  NT CE is higher over the entire wavelength region. This is consistent with the achieved  $J_{sc}$  value. The significant increase in IPCE further verified that  $\text{CuAgSe}$  NTs possessed both super catalytic activity and high electrical conductivity. To understand the improved QDSSC performance, EIS and Tafel polarization measurements were performed on dummy cells assembled with two identical electrodes. Figure 6c shows the Nyquist plots of the dummy cells with different CEs. The inset equivalent circuit includes  $R_s$ ,  $R_{ct}$ , and  $Z_w$ . A smaller resistance means better electrocatalytic activity of the CEs.<sup>[40–42]</sup> The  $R_s$  value of the  $\text{CuAgSe}$  CE ( $10.8 \Omega$ ) is smaller than those of the  $\text{Cu}_{2-x}\text{Se}$  ( $12.9 \Omega$ ) and Au ( $16.0 \Omega$ ) CEs, which indicates the superior electrical conductivity of  $\text{CuAgSe}$ . Moreover, the  $\text{CuAgSe}$  CE has the smallest  $R_{ct}$  value ( $0.67 \Omega$ ; compared with  $\text{Cu}_{2-x}\text{Se}$  ( $0.81 \Omega$ ) and Au ( $42.43 \Omega$ ) CEs), which means that the  $\text{CuAgSe}$  CE has the best electrocatalytic activity towards the reduction of polysulfide among the three CEs. This is consistent with the  $J_{sc}$  values in the order of the  $\text{CuAgSe}$  ( $17.57 \text{ mA cm}^{-2}$ ) >  $\text{Cu}_{2-x}\text{Se}$  ( $17.13 \text{ mA cm}^{-2}$ ) > Au ( $13.34 \text{ mA cm}^{-2}$ ) CEs. The smallest  $Z_w$  value of the  $\text{CuAgSe}$  CE ( $4.17 \Omega$ ) reveals efficient diffusion of

the polysulfide electrolyte. The highest FF value for the QDSSCs with the CuAgSe CE can be attributed to the smallest  $Z_w$  and  $R_s$  values. Figure 6d shows the logarithmic current density ( $\log J$ ) as a function of the voltage ( $V$ ) for the oxidation/reduction of polysulfide to form sulfide. The slopes for the anodic and cathodic branches are in the order of CuAgSe NTs > Cu<sub>2-x</sub>Se NTs > Au. The larger slope for the CuAgSe NT indicates a larger exchange current density, which is consistent with the EIS results. Better electrochemical performance of the CuAgSe CE compared with that of the Cu<sub>2-x</sub>Se CE is due to the higher mobility of both Cu<sup>+</sup> and Ag<sup>+</sup> ions in the CuAgSe NTs. The electrical conductivity of a single NT, to provide direct evidence for comparison of the electrical performances of these two NTs, will be measured and reported in our next study. The higher conversion efficiency of QDSSCs from ternary and binary NT-based CEs is attributed to the higher stability of metal selenides in polysulfide electrolyte than that of the Au CE because good conductivity is retained by avoiding corrosion and passivation.

The superior electrical conductivity and electrocatalytic activity of CuAgSe NTs relative to Cu<sub>2-x</sub>Se NTs led to an enhancement in power conversion efficiency of QDSSCs made with CuAgSe CE ( $\eta = 5.61\%$ ) in comparison with that made with Cu<sub>2-x</sub>Se CE ( $\eta = 5.19\%$ ), although this is not the highest record for QDSSCs.<sup>[43–46]</sup> It should be noted that these values are lower than those in our previous reports because the photoelectrodes used herein are made from commercial TiO<sub>2</sub> nanoparticles rather than porous TiO<sub>2</sub> nanosheets, which could effectively scatter the incident light and improve the conversion efficiency.<sup>[47]</sup> The use of commercial TiO<sub>2</sub> nanoparticles would be important for evaluating the practical application of our 1D/2D CuAgSe NTs.

## Conclusion

One-/two-dimensional pure ternary CuAgSe NTs were successfully prepared from Cu<sub>2-x</sub>Se NTs by cation exchange with silver nitrate (or silver acetate) at room temperature within a short time. Fast cation exchange is due to the ionic characteristics of copper/silver chalcogenides, and the strong capability of copper and silver ions to diffuse into/out of the lattice. The CuAgSe NTs with a designed architecture were used to fabricate CEs for QDSSCs that showed better electrochemical performance and higher conversion efficiency ( $\eta = 5.61\%$ ) than those of the original Cu<sub>2-x</sub>Se NT CE ( $\eta = 5.19\%$ ) and Au CE ( $\eta = 3.32\%$ ). Our research not only opens up a new way to design more effective CE catalysts for highly efficient QDSSCs, but also provides a facile method to fabricate nanostructures of ternary selenides with specifically designed architectures for diverse applications.

## Experimental Section

### Chemicals

NaOH (97.0%, Alfa Aesar), Cu(NO<sub>3</sub>)<sub>2</sub>·3H<sub>2</sub>O (99.5%, Aldrich), ethylenediamine (99.0%, Alfa Aesar), hydrazine (35 wt% in H<sub>2</sub>O, Aldrich),

2-mercaptoethanol (>99.0%, Aldrich), selenium powder (–325 mesh, 99.5%, Alfa Aesar), silver nitrate (>99.0%, Sigma-Aldrich), silver acetate (>99.99%, Sigma-Aldrich), anhydrous ethanol (>99.5%, Sigma-Aldrich), acetone (>99.9%, Sigma-Aldrich), and Milli-Q water (18.2 MΩ·cm) were used as received.

### Synthesis of CuAgSe NTs

Cu<sub>2-x</sub>Se NTs were prepared as described elsewhere.<sup>[48]</sup> In a typical synthesis, as-prepared Cu<sub>2-x</sub>Se NTs (0.15 mmol) were dispersed in anhydrous ethanol (0.5 mL), followed by the addition of solutions (2.5 mL) of silver nitrate or silver acetate (0.15 mmol) in ethanol under gentle stirring for 20–40 min. The black precipitates were purified by rinsing with distilled water and ethanol several times, followed by drying at room temperature.

### Evolution of CuAgSe NTs

The evolution of NTs was investigated by characterizing samples collected at different reaction times. Two groups of experiments were performed. The first group of experiments were performed by using silver nitrate for the cation-exchange reaction, and the samples were collected at 1, 2, 10, and 20 min. The second group of experiments were conducted by using silver acetate for cation exchange, and the samples were collected at 1, 2, 10, 20, and 60 min.

### Characterization of nanostructures

Powder XRD patterns for all samples were collected by using Cu<sub>Kα1</sub> radiation ( $\lambda = 1.5406 \text{ \AA}$ ) at 40 kV and 25 mA with a position-sensitive detector. EDX, XPS, and ICP-AES measurements were used to characterize the chemical composition and crystal structure of the samples. The FE-SEM images of all the samples were collected by using a JEOL JMS 7500-FA microscope with an accelerating voltage of 5 kV and a secondary electron detector. The TEM images were collected on a JEOL ARM200F microscope operated at 200 kV.

### Preparation of photoelectrodes

CdS- and CdSe-sensitized TiO<sub>2</sub> working electrodes were prepared by successively casting the commercial TiO<sub>2</sub> pastes on fluorine-doped tin oxide (FTO) substrates by using the doctor blade technique. The TiO<sub>2</sub> film was composed of a 13.7 μm transparent layer (18NR-T paste, Dyesol). The working electrodes were gradually heated at 100 °C for 15 min and 500 °C for 30 min, respectively.<sup>[38]</sup>

### Preparation of CEs

The CuAgSe and Cu<sub>2-x</sub>Se electrodes were prepared on FTO substrates by the doctor blade technique with CuAgSe and Cu<sub>2-x</sub>Se pastes, respectively. The pastes were prepared from CuAgSe and Cu<sub>2-x</sub>Se powders according to a previous study with some modifications.<sup>[39]</sup> The newly formed films were annealed at 350 °C for 30 min in an argon atmosphere to remove the binder and enhance the contact between the film and substrate. For comparison, gold electrodes were prepared by sputtering to yield a thickness of approximately 50 nm (obtained from the calibration curve of the sputtering).

## Assembly and measurements of QDSSCs

The solar cells were fabricated by assembling the CE (CuAgSe, Cu<sub>2-x</sub>Se, and Au) and (QD-sensitized TiO<sub>2</sub> film electrode with a binder clip separated by a 60 μm thick spacer. A mask with a window area of 0.16 cm<sup>2</sup> was clipped onto the TiO<sub>2</sub> side to define the active area of the cell during testing. The polysulfide electrolyte was composed of 2 M Na<sub>2</sub>S, 2 M S, and 0.2 M KCl in Milli-Q water. For QDSSCs assembled under each set of conditions, at least eight cells were prepared and tested in parallel, and the one with the medium value was chosen for the final data. For EIS and Tafel polarization measurements, symmetric dummy cells were assembled from two identical CEs with the same polysulfide electrolyte. The active area of the dummy cells was 0.64 cm<sup>2</sup>. The *J*-*V* tests on the QDSSCs were performed under one sun conditions by using an air mass (AM) 1.5 solar simulator (Oriel), which was carefully calibrated with certified silicon solar cells. The light intensity of the solar simulator was adjusted to 100 mW cm<sup>-2</sup> by using an optical power meter (Newport, 1918-c) with a detector (818P-040-25). *J*-*V* curves were obtained by applying an external bias to the cell, and measurements were recorded by using a Keithley model 2420 digital source meter. The IPCE plotted as a function of the excitation wavelength was obtained by using a Newport 1918-c power meter under irradiation of a 300 W Oriel xenon light source with an Oriel Cornerstone 260 1/4m monochromator in direct-current mode. The EIS results were collected with dummy cells by using a Solartron 1260 frequency-response analyzer in combination with a Solartron 1480 potentiostat in the dark. The applied bias voltage and alternating current (ac) amplitude were set at 0 V and 10 mV, and the frequency ranged from 106 to 0.1 Hz. Then, the Tafel polarization measurements were performed at a scan rate of 20 mVs<sup>-1</sup> on an electrochemical workstation (CHI660d).

## Acknowledgements

X.Q.C. gratefully acknowledges funding from the Chinese Scholarship Council (CSC) (201206770014). Z.L. acknowledges support from the Australian Research Council (ARC) through the Discovery Projects DP130102699 and DP130102274, the Natural National Science Foundation of China through a project 81471657, Jiangsu Specially Appointed Professorship, and a Project Funded by the Priority Academic Program Development of Jiangsu Higher Education Institutions (PAPD). S.X.D. is grateful for support from the ARC through the Linkage Project LP120200289. We also appreciate support from the Electron Microscopy Centre at UOW (Linkage Infrastructure, Equipment and Facility Grant LE120100104 for JEOL JEM-ARM200F), and thank Dr. Tania Silver for critical reading of the manuscript and Dr. Dongqi Shi for carrying out XPS measurements.

**Keywords:** copper · electrochemistry · ion exchange · nanotubes · silver

- [1] J. Xu, C. S. Lee, Y. B. Tang, X. Chen, Z. H. Chen, W. J. Zhang, S. T. Lee, W. X. Zhang, Z. H. Yang, *ACS Nano* **2010**, *4*, 1845–1850.
- [2] W. T. Bi, M. Zhou, Z. Y. Ma, H. Y. Zhang, J. B. Yu, Y. Xie, *Chem. Commun.* **2012**, *48*, 9162–9164.
- [3] B. Mukherjee, A. Peterson, V. Subramanian, *Chem. Commun.* **2012**, *48*, 2415–2417.
- [4] C. M. Lieber, Z. L. Wang, *MRS Bull.* **2007**, *32*, 99–108.
- [5] G. Q. Zhang, B. Y. Xia, C. Xiao, L. Yu, X. Wang, Y. Xie, X. W. Lou, *Angew. Chem. Int. Ed.* **2013**, *52*, 8643–8647; *Angew. Chem.* **2013**, *125*, 8805–8809.
- [6] C. X. Fang, S. Y. Zhang, P. F. Zuo, W. Wei, B. K. Jin, J. Y. Wu, Y. P. Tian, *J. Cryst. Growth* **2009**, *311*, 2345–2351.
- [7] M. T. Neshkova, V. D. Nikolova, A. M. Bond, V. Petrov, *Electrochim. Acta* **2005**, *50*, 5606–5615.
- [8] S. J. Peng, T. R. Zhang, L. L. Li, C. Shen, F. Y. Cheng, M. Srinivasan, Q. Y. Yan, S. Ramakrishna, J. Chen, *Nano Energy* **2015**, *16*, 163–172.
- [9] J. W. Earley, *Am. Mineral.* **1950**, *35*, 345–347.
- [10] A. J. Frueh, G. K. Czamanke, C. H. Knight, *Z. Kristallogr.* **1957**, *108*, 389–396.
- [11] S. Ishiwata, Y. Shiomi, J. S. Lee, M. S. Bahramy, T. Suzuki, M. Uchida, R. Arita, Y. Taguchi, Y. Tokura, *Nat. Mater.* **2013**, *12*, 512–517.
- [12] A. J. Hong, T. Li, H. X. Zhu, X. H. Zhou, Q. Y. He, W. S. Liu, Z. B. Yan, J. M. Liu, Z. F. Ren, *Solid State Ionics* **2014**, *261*, 21–25.
- [13] R. B. Baikulov, Y. G. Asadov, *Inorg. Mater.* **2005**, *41*, 338–342.
- [14] C. Han, Q. Sun, Z. X. Cheng, J. L. Wang, Z. Li, G. Q. Lu, S. X. Dou, *J. Am. Chem. Soc.* **2014**, *136*, 17626–17633.
- [15] Y. H. Gao, Z. Zheng, Y. P. Tian, Y. D. Zhang, Y. G. Zhang, *Eur. J. Inorg. Chem.* **2011**, 4198–4203.
- [16] S. Gupta, S. V. Kershaw, A. L. Rogach, *Adv. Mater.* **2013**, *25*, 6923–6943.
- [17] D. H. Ha, A. H. Caldwell, M. J. Ward, S. Honrao, K. Mathew, R. Hovden, M. A. Koker, D. A. Muller, H. G. Hennig, R. D. Robinson, *Nano Lett.* **2014**, *14*, 7090–7099.
- [18] W. van der Stam, Q. A. Akkerman, X. X. Ke, M. A. Huis, S. Bals, C. M. Donega, *Chem. Mater.* **2015**, *27*, 283–291.
- [19] L. De Trizio, H. B. Li, A. Casu, A. Genovese, A. Sathya, G. C. Messina, L. Manna, *J. Am. Chem. Soc.* **2014**, *136*, 16277–16284.
- [20] D. H. Son, S. M. Hughes, Y. D. Yin, A. P. Alivisatos, *Science* **2004**, *306*, 1009–1012.
- [21] I. Kriegl, J. Rodriguez-Fernandez, A. Wisnet, H. Zhang, C. Waurisch, A. Eychmuller, A. Dubavik, A. O. Govorov, J. Feldmann, *ACS Nano* **2013**, *7*, 4367–4377.
- [22] S. L. Xiong, H. C. Zeng, *Angew. Chem. Int. Ed.* **2012**, *51*, 949–952; *Angew. Chem.* **2012**, *124*, 973–976.
- [23] X. J. Wu, X. Huang, J. Q. Liu, H. Li, J. Yang, B. Li, W. Huang, H. Zhang, *Angew. Chem. Int. Ed.* **2014**, *53*, 5083–5087; *Angew. Chem.* **2014**, *126*, 5183–5187.
- [24] R. D. Robinson, B. Sadtler, D. O. Demchenko, C. K. Erdonmez, L. W. Wang, A. P. Alivisatos, *Science* **2007**, *317*, 355–358.
- [25] J. Y. Tang, Z. Y. Huo, S. Brittman, H. W. Gao, P. D. Yang, *Nat. Nanotechnol.* **2011**, *6*, 568–572.
- [26] H. B. Li, R. Brescia, R. Krahne, G. Bertoni, M. J. P. Alcocer, C. D'Andrea, F. Scotognella, F. Tassone, M. Zanella, M. De Giorgi, L. Manna, *ACS Nano* **2012**, *6*, 1637–1647.
- [27] H. B. Li, R. Brescia, M. Povia, M. Prato, G. Bertoni, L. Manna, I. Moreels, *J. Am. Chem. Soc.* **2013**, *135*, 12270–12278.
- [28] D. D. Zhang, A. B. Wong, Y. Yu, S. Brittman, J. W. Sun, A. Fu, B. Beberwyck, A. P. Alivisatos, P. D. Yang, *J. Am. Chem. Soc.* **2014**, *136*, 17430–17433.
- [29] K. Miszta, R. Brescia, M. Prato, G. Bertoni, S. Marras, Y. Xie, S. Ghosh, M. R. Kim, L. Manna, *J. Am. Chem. Soc.* **2014**, *136*, 9061–9069.
- [30] S. C. Riha, D. C. Johnson, A. L. Prieto, *J. Am. Chem. Soc.* **2011**, *133*, 1383–1390.
- [31] X. Q. Chen, Z. Li, J. P. Yang, Q. Sun, S. X. Dou, *J. Colloid Interface Sci.* **2015**, *442*, 140–146.
- [32] L. W. Mi, W. T. Wei, Z. Zheng, G. S. Zhu, H. W. Hou, W. H. Chen, X. X. Guan, *Nanoscale* **2014**, *6*, 1124–1133.
- [33] X. Q. Chen, Z. Li, S. X. Dou, *ACS Appl. Mater. Interfaces* **2015**, *7*, 13295–13302.
- [34] V. Lesnyak, R. Brescia, G. C. Messina, L. Manna, *J. Am. Chem. Soc.* **2015**, *137*, 9315–9323.
- [35] F. Grønvdal, S. Stolen, Y. Semenov, *Thermochim. Acta* **2003**, *399*, 213–224.
- [36] K. C. Mills, *Thermodynamic Data for Inorganic Sulphides, Selenides and Tellurides*, Butterworths, London, **1974**.
- [37] C. W. Liu, Z. L. Qiu, F. Li, W. L. Meng, W. J. Yue, F. P. Zhang, Q. Q. Qiao, M. T. Wang, *Nano Energy* **2015**, *12*, 686–697.
- [38] Y. Bai, H. Yu, Z. Li, R. Amal, G. Q. Lu, L. Z. Wang, *Adv. Mater.* **2012**, *24*, 5850–5856.



- [39] Y. Bai, C. Han, X. Q. Chen, H. Yu, X. Zong, Z. Li, L. Z. Wang, *Nano Energy* **2015**, *13*, 609–619.
- [40] J. K. Lee, D. Y. Son, T. K. Ahn, H. W. Shin, I. Y. Kim, S. J. Hwang, M. J. Ko, S. Sul, H. Han, N. G. Park, *Sci. Rep.* **2013**, *3*, 1–8.
- [41] P. K. Santra, P. V. Kamat, *J. Am. Chem. Soc.* **2012**, *134*, 2508–2511.
- [42] M. X. Wu, X. A. Lin, A. Hagfeldt, T. L. Ma, *Angew. Chem. Int. Ed.* **2011**, *50*, 3520–3524; *Angew. Chem.* **2011**, *123*, 3582–3586.
- [43] J. Wang, I. Mora-Sero, Z. X. Pan, K. Zhao, H. Zhang, Y. Y. Feng, G. Yang, X. H. Zhong, J. Bisquert, *J. Am. Chem. Soc.* **2013**, *135*, 15913–15922.
- [44] Z. X. Pan, I. Mora-Sero, Q. Shen, H. Zhang, Y. Li, K. Zhao, J. Wang, X. H. Zhong, J. Bisquert, *J. Am. Chem. Soc.* **2014**, *136*, 9203–9210.
- [45] S. Jiao, Q. Shen, I. Mora-Sero, J. Wang, Z. X. Pan, K. Zhao, Y. Kuga, X. H. Zhong, J. Bisquert, *ACS Nano* **2015**, *9*, 908–915.
- [46] K. Zhao, Z. X. Pan, I. Mora-Sero, E. Canovas, H. Wang, Y. Song, X. Q. Gong, J. Wang, M. Bonn, J. Bisquert, X. H. Zhong, *J. Am. Chem. Soc.* **2015**, *137*, 5602–5609.
- [47] T. G. Deepak, G. S. Anjusree, S. Thomas, T. A. Arun, S. V. Nair, A. S. Nair, *RSC Adv.* **2014**, *4*, 17615–17638.
- [48] X. Q. Chen, Z. Li, Y. Bai, Q. Sun, L. Z. Wang, S. X. Dou, *Chem. Eur. J.* **2015**, *21*, 1055–1063.

---

Manuscript received: October 8, 2015


Revised: November 23, 2015

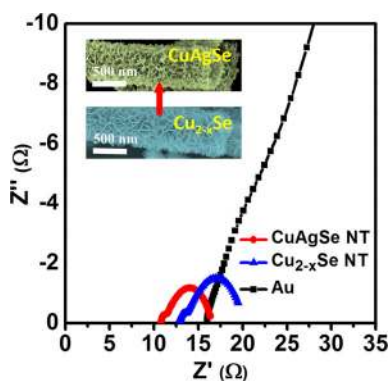
Final Article published: ■ ■ ■, 0000

## FULL PAPERS

X. Q. Chen, Y. Bai, Z. Li,\* L. Z. Wang,  
S. X. Dou



 Ambient Synthesis of One-/Two-Dimensional CuAgSe Ternary Nanotubes as Counter Electrodes of Quantum-Dot-Sensitized Solar Cells



**Metal exchange:** One-/two-dimensional CuAgSe nanotubes are prepared from  $\text{Cu}_{2-x}\text{Se}$  nanotubes by a cation-exchange approach and explored as counter electrodes in quantum-dot-sensitized solar cells to achieve high conversion efficiency (see figure).